

Uncertainty-Weighted Multi-Task CNN for Joint DoA and Rain-Rate Estimation Under Rain-Induced Array Distortions

Chenyang Yan^{*○}, Ruonan Yang^{†○}, Shunqiao Sun[†], and Mats Bengtsson^{*}

[○]These authors contributed equally to this work.

^{*}KTH Royal Institute of Technology, Stockholm, Sweden

[†]The University of Alabama, Tuscaloosa, AL USA

Abstract—We investigate joint direction-of-arrival (DoA) and rain-rate estimation for a uniform linear array operating under rain-induced multiplicative distortions. Building on a waveform fluctuation model whose spatial correlation is governed by the rain-rate, we derive an angle-dependent covariance formulation and use it to synthesize training data. DoA estimation is cast as a multi-label classification problem on a discretized angular grid, while rain-rate estimation is formulated as a multi-class classification task. We then propose a multi-task deep CNN with a shared feature extractor and two task-specific heads, trained using an uncertainty-weighted objective to automatically balance the two losses. Numerical results in a two-source scenario show that the proposed network achieves lower DoA RMSE than classical baselines and provides accurate rain-rate classification at moderate-to-high SNRs.

Index Terms—Direction-of-arrival estimation, multi-task learning, uncertainty weighting, convolutional neural networks, covariance-based learning.

I. INTRODUCTION

Direction-of-arrival (DoA) estimation is a key enabler for radar-based autonomous driving and obstacle detection [1]–[3]. Under heavy rain, propagation effects such as attenuation and backscattering distort array measurements and can substantially degrade DoA performance, especially in multi-source localization [4], [5].

In our previous work, we developed a physics-based rain-impaired array model and a covariance-matching calibration method [6] based on [7]. However, the distortion should be angle-dependent and the analysis was restricted to the single-source case. Moreover, since the distortion statistics are governed by the rain-rate, jointly estimating the rain-rate alongside DoA is both feasible and practically useful as an auxiliary environmental indicator.

Motivated by recent learning-based DoA estimators that show improved robustness under low SNR, model mismatch,

[○]Chenyang Yan and Ruonan Yang contributed equally to this work (co-first authors).

The work of R. Yang and S. Sun was supported in part by U.S. National Science Foundation (NSF) under Grants CCF-2153386 and ECCS-2033433. The computations were partly enabled by resources provided by the National Academic Infrastructure for Supercomputing in Sweden (NAIIS), partially funded by the Swedish Research Council through grant agreement no. 2022-06725.

and complex environments [8]–[13], we propose a multi-task deep CNN that learns DoA and rain-rate information directly from covariance measurements under rain-induced distortions.

The contributions of this paper are summarized as follows:

- We propose a CNN-based framework for joint DoA and rain-rate estimation under a rain-impaired array measurement model, and validate it in a two-source scenario.
- We develop an uncertainty-weighted multi-task objective that automatically balances the DoA and rain-rate classification losses during training.
- Experiments under rain-induced distortions demonstrate the potential advantages of deep learning-based joint estimation over classical baselines in challenging conditions.

II. RAIN-INDUCED DISTORTION AND SIGNAL MODEL

This section presents the rain-induced distortion model and its resulting array signal formulation. We first describe the waveform-level fluctuation statistics of the complex electric field and introduce an empirical correlation model parameterized by the rain-rate. We then map the waveform distortions to a multiplicative array observation model and extend it to the multi-source ULA case with angle-dependent distortions. Finally, we lift the model to the covariance domain, where the rain-rate information is embedded in the distortion covariance $\mathbf{R}_b(\theta)$ through a correlation coefficient α , providing the basis for subsequent joint DoA and rain-rate estimation.

A. Rain-Induced Distortion Model

Following the rain-induced waveform fluctuation model in [7], let P denote a point on the received waveform. For a given rain realization, let $E(P) \in \mathbb{C}$ denote the complex electric-field envelope at P . The mean (coherent) field is defined as $E_{\text{mean}}(P) \triangleq \mathbb{E}\{E(P)\}$, where $\mathbb{E}\{\cdot\}$ denotes the ensemble average over independent rain realizations. The normalized electric-field fluctuation is defined as

$$E_n(P) \triangleq \frac{E(P) - E_{\text{mean}}(P)}{E_{\text{mean}}(P)}. \quad (1)$$

Consider two points P_1 and P_2 on the same waveform with separation d , and define $E_{n,1} \triangleq E_n(P_1)$ and $E_{n,2} \triangleq E_n(P_2)$.

We model $E_{n,1}$ and $E_{n,2}$ as zero-mean, jointly circularly symmetric complex Gaussian random variables with second-order statistics:

$$\mathbb{E}\{|E_{n,1}|^2\} = \mathbb{E}\{|E_{n,2}|^2\} = 2\lambda_{11}, \quad (2)$$

$$\mathbb{E}\{E_{n,1}E_{n,2}^*\} = 2\alpha\lambda_{11}, \quad \Im\{\mathbb{E}\{E_{n,1}E_{n,2}^*\}\} = 0, \quad (3)$$

where λ_{11} controls the fluctuation power and α characterizes the spatial correlation on the wavefront. The parameter α depends on the rain-rate, propagation distance, separation d , and radar carrier frequency, and can be computed using the empirical model in Eq. (13) of [7]:

$$\alpha = \exp\left(-a_1\left(\frac{R}{a_2R+1}\right)\left(\frac{\frac{d}{\lambda_0}}{a_3\frac{d}{\lambda_0}+1}\right)\right), \quad (4)$$

where R denotes the propagation range, λ_0 is the wavelength, and a_1 , a_2 , and a_3 are parameters determined by the rain-rate and carrier frequency (see Table II in [7]). According to [7], (4) is valid for $R \leq 500$ m and $0.1 \leq d/\lambda_0 \leq 8$. The probability density functions (pdfs) of the phase difference and magnitude ratio under varying parameters (e.g., separation d , range, and rain-rate) are illustrated in Figs. 1 and 2 of [6].

B. Array Observation Model

We now connect the wavefront model to array observations. Consider a uniform linear array (ULA) with M sensors. Let P_m denote the location of the m th sensor, and identify the received signal $y_m(t)$ with the complex electric field $E(P_m, t)$. Substituting (1) yields

$$y_m(t) = (1 + E_n(P_m, t)) E_{\text{mean}}(P_m), \quad (5)$$

where $E_{\text{mean}}(P_m)$ denotes the mean field component, i.e., the distortion-free received field at P_m . Accordingly, we define the multiplicative distortion at sensor m as

$$b_m(t) \triangleq 1 + E_n(P_m, t). \quad (6)$$

Note that this definition differs from our previous implementation in [6], where the distortion term was taken as $b_m(t) = E_n(P_m, t)$. This difference corresponds to a reparameterization that absorbs the constant offset into the distortion coefficient; therefore, the subsequent modeling and the proposed algorithm remain applicable under (6).

In [6], we introduced a rain-impaired array reception model in which the complex electric-field fluctuations occur across the incident plane wave as it reaches the ULA aperture (see Fig. 3 in [6]). For the single-source case, the corresponding covariance model was derived in Eq. (9) of [6], where the rain-induced distortion appears as a Hadamard product between the distortion-free covariance matrix and a real Toeplitz distortion matrix \mathbf{R}_b , defined in Eq. (10) of [6].

Starting from Eq. (5) in [6], we extend the model to N narrowband sources, where the n th source impinges from direction θ_n . The measurement model of a rain-distorted ULA is then given by

$$\mathbf{y}(t) = \sum_{n=1}^N \left[\mathbf{a}(\theta_n) \odot \mathbf{b}(\theta_n, t) \right] s_n(t) + \mathbf{n}(t), \quad (7)$$

where $\mathbf{y}(t) \in \mathbb{C}^M$ denotes the received array snapshot, $\mathbf{a}(\theta_n) \in \mathbb{C}^M$ is the distortion-free steering vector, $s_n(t) \in \mathbb{C}$ is the n th source signal, and $\mathbf{n}(t) \in \mathbb{C}^M$ denotes additive noise. The vector $\mathbf{b}(\theta_n, t) \in \mathbb{C}^M$ represents the multiplicative rain-induced distortion affecting the n th wavefront across the array and is defined as

$$\mathbf{b}(\theta_n, t) \triangleq [b_{n,1}(t), b_{n,2}(t), \dots, b_{n,M}(t)]^T, \quad (8)$$

where $b_{n,m}(t)$ denotes the distortion coefficient at sensor m associated with the wavefront arriving from direction θ_n .

The distortion vector $\mathbf{b}(\theta_n, t)$ is angle-dependent because the effective separation on the reference wavefront plane (see Fig. 3 in [6]) varies with the incidence angle. In particular, for an inter-element spacing d_0 in wavelength along the array axis, the corresponding inter-element spacing in wavelength on the wavefront is

$$d(\theta_n) = d_0 \cos(\theta_n). \quad (9)$$

Hence, the correlation parameter α (and thus the statistics of $\mathbf{b}(\theta_n, t)$) inherits an explicit dependence on θ_n through $d(\theta_n)$.

C. Covariance-Domain Formulation

Alternatively, (7) can be lifted to the covariance domain. Define the source vector $\mathbf{s}(t) \triangleq [s_1(t), \dots, s_N(t)]^T \in \mathbb{C}^N$ and the DoA collection $\boldsymbol{\theta} \triangleq [\theta_1, \dots, \theta_N]^T$. We assume that $\mathbf{s}(t)$ and $\mathbf{n}(t)$ are independent, zero-mean, circularly symmetric complex processes. Moreover, we assume mutually uncorrelated sources with equal power, such that

$$\mathbf{R}_s \triangleq \mathbb{E}\{\mathbf{s}(t)\mathbf{s}(t)^H\} = \sigma_s^2 \mathbf{I}_N, \quad \mathbf{R}_n \triangleq \mathbb{E}\{\mathbf{n}(t)\mathbf{n}(t)^H\}, \quad (10)$$

where σ_s^2 denotes the per-source signal power and \mathbf{I}_N is the $N \times N$ identity matrix. Under these assumptions, the covariance matrix of $\mathbf{y}(t)$ is given by

$$\begin{aligned} \mathbf{R}_y &\triangleq \mathbb{E}\{\mathbf{y}(t)\mathbf{y}(t)^H\} \\ &= \sum_{n=1}^N \left[\mathbf{R}_x(\theta_n) \odot \mathbf{R}_b(\theta_n) \right] + \mathbf{R}_n, \end{aligned} \quad (11)$$

where $\mathbf{R}_x(\theta_n)$ denotes the distortion-free array covariance contribution of the n th source,

$$\mathbf{R}_x(\theta_n) = \sigma_s^2 \mathbf{a}(\theta_n) \mathbf{a}(\theta_n)^H. \quad (12)$$

The matrix $\mathbf{R}_b(\theta_n) \in \mathbb{C}^{M \times M}$ is the rain-induced distortion covariance associated with direction θ_n , defined elementwise as

$$[\mathbf{R}_b(\theta_n)]_{m\ell} \triangleq \mathbb{E}\{b_{n,m}(t) b_{n,\ell}^*(t)\}, \quad 1 \leq m, \ell \leq M. \quad (13)$$

Using $b_{n,m}(t) = 1 + E_n(P_m, t)$ and the second-order statistics of $E_n(\cdot)$, we obtain

$$[\mathbf{R}_b(\theta_n)]_{m\ell} = \begin{cases} 1 + 2\lambda_{11}, & m = \ell, \\ 1 + 2\lambda_{11} \alpha_{m\ell}(\theta_n), & m \neq \ell, \end{cases} \quad (14)$$

where $\alpha_{m\ell}(\theta_n)$ denotes the correlation parameter corresponding to the sensor-pair separation. In particular, $\alpha_{m\ell}(\theta_n)$ is evaluated by (4) with

$$d = |m - \ell| d(\theta_n), \quad d(\theta_n) = d_0 \cos(\theta_n). \quad (15)$$

Hence, $\mathbf{R}_b(\theta_n)$ inherits an explicit dependence on θ_n through the angle-dependent separation $d(\theta_n)$. Moreover, since $\alpha_{ml}(\theta_n)$ is computed via (4), the rain-rate information is fully captured by $\mathbf{R}_b(\theta_n)$ (through a_1 , a_2 , and a_3) and propagates to the observed covariance \mathbf{R}_y in (11).

III. PROPOSED METHOD

In this section, we formulate DoA estimation as a multi-label classification task and rain-rate estimation as a multi-class classification task. We then develop a multi-task CNN architecture that jointly learns these tasks from the sample covariance matrix \mathbf{R}_y , thereby exploiting both DoA- and rain-rate-dependent information embedded in the covariance measurements.

A. Input Representation and Preprocessing

Following [9], we cast DoA prediction as a multi-label classification task over a discretized angular grid. Specifically, the search interval $[-\theta_{\max}, \theta_{\max}]$ is uniformly quantized with resolution ρ to form the grid \mathcal{G} . The DoA label is encoded as a binary vector over \mathcal{G} , where the entries corresponding to the true source angles are set to one and all other entries are set to zero.

For rain-rate classification, we consider six discrete classes. Following Table II in [7], we use five rain-rate levels $\{2, 5, 10, 25, 50\}$ mm/h and add an additional no-rain class (0 mm/h), for which no rain-induced distortion is applied (i.e., the distortion coefficients are set to unity). For each rain-rate class, the corresponding distortion covariance is constructed from (14). We then synthesize spatially correlated complex Gaussian distortion samples by transforming i.i.d. Gaussian draws with a Cholesky factor of the target covariance (a square-root covariance transformation) [14]. These samples are used to generate rain-distorted covariance measurements for training.

For each training example, we compute the sample covariance matrix $\hat{\mathbf{R}}_y$ from the received snapshots and construct a real-valued three-channel input tensor $\mathbf{X} \in \mathbb{R}^{M \times M \times 3}$, whose channels are $\Re\{\hat{\mathbf{R}}_y\}$, $\Im\{\hat{\mathbf{R}}_y\}$, and $\angle\{\hat{\mathbf{R}}_y\}$, respectively [9]. Here, $\Re\{\cdot\}$ and $\Im\{\cdot\}$ denote the real and imaginary parts of a complex matrix, and $\angle\{\cdot\}$ denotes the phase (argument) of a complex-valued entry.

B. Network Architecture

The nonlinear mapping $f(\cdot)$ is parameterized by a deep convolutional neural network (CNN) comprising a shared feature extractor and task-specific prediction heads. Let $\mathbf{X} \in \mathbb{R}^{M \times M \times 3}$ denote the input tensor constructed from the sample covariance matrix, where the three channels contain the real part, imaginary part, and phase, respectively. The network first applies a cascade of four convolutional blocks:

$$f(\mathbf{X}) = f_4(f_3(f_2(f_1(\mathbf{X}))). \quad (16)$$

These four convolutional blocks collectively constitute a shared CNN encoder. Each block $f_i(\cdot)$, $i \in \{1, 2, 3, 4\}$, consists of a 2-D convolution with $n_C = 256$ filters, followed

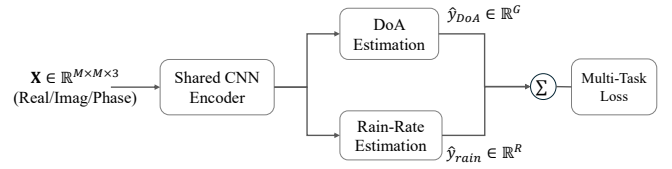


Fig. 1: Proposed multi-task network for joint DoA and rain-rate estimation. The input tensor $\mathbf{X} \in \mathbb{R}^{M \times M \times 3}$ stacks the real, imaginary, and phase channels of the sample covariance matrix and is processed by a shared CNN encoder. Two task-specific heads output DoA logits $\hat{y}_{\text{DoA}} \in \mathbb{R}^G$ and rain-rate logits $\hat{y}_{\text{rain}} \in \mathbb{R}^R$, which are jointly optimized via a multi-task loss.

by batch normalization and a rectified linear unit (ReLU). All convolutions use a 3×3 kernel with stride 1 and padding 1. A 2×2 max-pooling layer with stride 2 is inserted after the second block $f_2(\cdot)$. The output feature maps after $f_4(\cdot)$ are then flattened into a feature vector.

The resulting feature vector is fed to a fully connected layer with 256 hidden units and ReLU activation, followed by a linear output layer that produces the DoA logits $\hat{y}_{\text{DoA}} \in \mathbb{R}^G$, where G is the number of angular grid points. In parallel, a task-specific rain-rate head with the same two-layer fully connected structure outputs the rain-rate logits $\hat{y}_{\text{rain}} \in \mathbb{R}^R$, where R denotes the number of rain-rate classes. During training, the DoA logits are converted to independent Bernoulli probabilities via a sigmoid and optimized using a multi-label binary cross-entropy (BCE) loss, whereas the rain-rate logits are converted to a categorical distribution via a softmax and optimized using cross-entropy (CE). In practice, these nonlinearities are applied implicitly within the respective loss functions. Finally, we associate each task with a learnable log-variance parameter, which is used for uncertainty-based reweighting of the multi-task objective. The structure of the network can be seen in Fig. 1

C. Multi-Task Learning with Uncertainty Weighting

The proposed network takes the covariance-based input \mathbf{X} and outputs two sets of logits: $\hat{y}_{\text{DoA}} \in \mathbb{R}^G$ for multi-label DoA prediction over the grid \mathcal{G} and $\hat{y}_{\text{rain}} \in \mathbb{R}^R$ for multi-class rain-rate prediction. To automatically balance the two tasks during training, we adopt uncertainty weighting [15].

Let $\mathbf{y}_{\text{DoA}} \in \{0, 1\}^G$ denote the multi-label DoA target and $y_{\text{rain}} \in \{1, \dots, R\}$ denote the rain-rate class label. We associate each task with a learnable scale parameter, $\sigma_{\text{DoA}} > 0$ and $\sigma_{\text{rain}} > 0$. We model the G binary labels as conditionally independent Bernoulli variables with scaled logits. Specifically, defining the element-wise sigmoid as $g(\cdot)$, we write

$$p(\mathbf{y}_{\text{DoA}} \mid \mathbf{X}, \mathbf{W}, \sigma_{\text{DoA}}) = \prod_{g=1}^G \left[g\left(\hat{y}_{\text{DoA},g} / \sigma_{\text{DoA}}^2\right)^{y_{\text{DoA},g}} \right. \\ \left. \times \left(1 - g\left(\hat{y}_{\text{DoA},g} / \sigma_{\text{DoA}}^2\right)\right)^{1-y_{\text{DoA},g}} \right]. \quad (17)$$

The corresponding negative log-likelihood reduces to a binary cross-entropy loss in logit form, where the DoA logits are scaled by $1/\sigma_{\text{DoA}}^2$. In other words, we compute the multi-label BCE loss using the scaled logits $\hat{\mathbf{y}}_{\text{DoA}}/\sigma_{\text{DoA}}^2$ and the target vector \mathbf{y}_{DoA} . The unscaled DoA loss is obtained by evaluating the same BCE on the original logits $\hat{\mathbf{y}}_{\text{DoA}}$. Throughout this section, the scaled loss is expressed as $\mathcal{L}_{\text{task}}(\mathbf{W}, \sigma_{\text{task}})$ and the unscaled loss is expressed as $\mathcal{L}_{\text{task}}(\mathbf{W})$.

Following the approximation used for classification in [15], the effect of temperature scaling can be expressed as a weighted unscaled loss plus a scale-dependent regularizer. Summing over the G independent Bernoulli factors yields

$$\mathcal{L}_{\text{DoA}}(\mathbf{W}, \sigma_{\text{DoA}}) \approx \frac{1}{\sigma_{\text{DoA}}^2} \mathcal{L}_{\text{DoA}}(\mathbf{W}) + G \log \sigma_{\text{DoA}}. \quad (18)$$

For rain-rate prediction we use the standard softmax cross-entropy loss $\mathcal{L}_{\text{rain}}(\mathbf{W}) = \ell_{\text{CE}}(\hat{\mathbf{y}}_{\text{rain}}, \mathbf{y}_{\text{rain}})$. Its uncertainty-weighted form is adopted directly from [15]:

$$\mathcal{L}_{\text{rain}}(\mathbf{W}, \sigma_{\text{rain}}) \approx \frac{1}{\sigma_{\text{rain}}^2} \mathcal{L}_{\text{rain}}(\mathbf{W}) + \log \sigma_{\text{rain}}. \quad (19)$$

For numerical stability, we optimize the log-variances $s_{\text{DoA}} = \log \sigma_{\text{DoA}}^2$ and $s_{\text{rain}} = \log \sigma_{\text{rain}}^2$. Combining (18) and (19) gives

$$\begin{aligned} \mathcal{L}(\mathbf{W}, s_{\text{DoA}}, s_{\text{rain}}) = & e^{-s_{\text{DoA}}} \mathcal{L}_{\text{DoA}}(\mathbf{W}) + e^{-s_{\text{rain}}} \mathcal{L}_{\text{rain}}(\mathbf{W}) \\ & + \frac{G}{2} s_{\text{DoA}} + \frac{1}{2} s_{\text{rain}}. \end{aligned} \quad (20)$$

IV. EVALUATION AND RESULTS

For training, we discretize the DoA space using a 1° grid over a field of view (FoV) of 60° centered at 0°, i.e., $\mathcal{G} = \{-30^\circ, -29^\circ, \dots, 30^\circ\}$, which yields a grid size of $G = 61$. We consider a fixed two-source scenario ($N = 2$) and fix the propagation range to $R = 200$ m. We then generate covariance samples uniformly across the six rain-rate classes described above and five SNR levels $\{0, 5, 10, 15, 20\}$ dB. In total, 100,000 samples are generated for training. The dataset is randomly split into a training set (90%) and a validation set (10%).

To evaluate the effect of multi-task loss weighting, we further compare the proposed uncertainty-weighted network with fixed loss weighting using a predefined ratio α , where the overall training loss is given by $\mathcal{L} = \mathcal{L}_{\text{DoA}} + \alpha \mathcal{L}_{\text{rain}}$. Results are reported for $\alpha = 1$ and $\alpha = 0.05$, enabling a direct comparison between the proposed adaptive weighting and fixed loss-weighting schemes.

Fig. 2 compares the DoA root-mean-square error (RMSE) of the proposed network with classical baselines, including MUSIC, root-MUSIC, ESPRIT, and MVDR, on the same test set consisting of 10,000 samples. In addition to outperforming the model-based methods, the proposed uncertainty-weighted network consistently improves upon its fixed-weighting variants across all SNRs. The benefit is most evident in the low-SNR regime, where uncertainty weighting yields noticeably lower RMSE, indicating that adaptive task balancing leads to more robust DoA inference under noisy and rain-distorted measurements. Table I compares the rain-rate classification

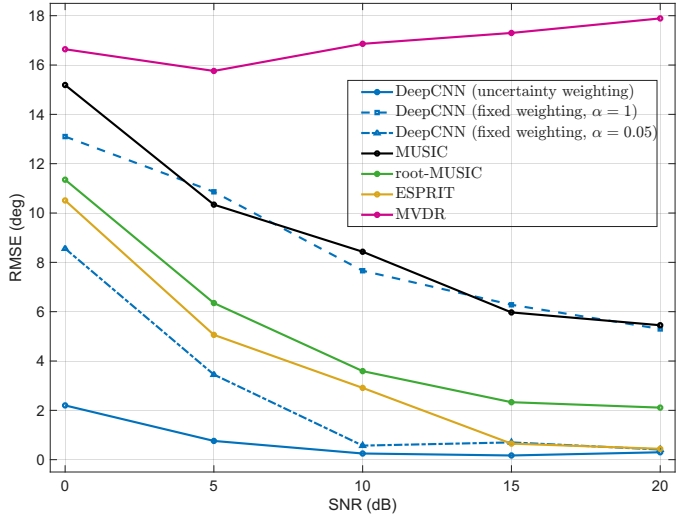


Fig. 2: DoA RMSE versus SNR on the test set under rain-induced array distortions. The proposed uncertainty-weighted network is compared with its fixed-weighting variants and classical baselines.

accuracy of the proposed uncertainty-weighted network with fixed-weighting variants. The proposed model consistently attains $\geq 94\%$ rain-rate classification accuracy across all tested SNR levels, indicating reliable rain-rate inference even in low-SNR conditions. Overall, the proposed uncertainty-weighted network achieves reliable performance on both DoA estimation and rain-rate classification in a unified multi-task framework.

TABLE I: Rain-rate classification accuracy (%) versus SNR for different loss weighting strategies.

SNR (dB)	Uncertainty weighting (see (20))	Fixed weighting	
		$\alpha = 0.05$	$\alpha = 1$
0	94.21	63.95	87.13
5	94.55	78.09	95.19
10	96.07	92.80	99.09
15	96.79	99.16	99.95
20	99.41	99.85	99.95

V. CONCLUSIONS

This paper proposes a CNN-based multi-task framework for jointly estimating the DoA and the rain-rate under rain-induced array distortions. The results provide initial evidence that the proposed formulation is feasible and can outperform classical DoA estimators in the considered setting. In addition, we extend uncertainty-weighted multi-task learning to a multi-label (sigmoid) DoA loss with a multi-class (softmax) rain-rate loss, yielding a principled and learnable mechanism to balance the two objectives.

Future work will validate the approach using real-world radar measurements, extend the current discrete rain-rate classifier to a continuous (regression) formulation, and investigate more challenging scenarios with a larger (and possibly varying) number of simultaneously active sources, including cases where the source count is unknown.

REFERENCES

- [1] S. Sun, A. P. Petropulu, and H. V. Poor, "MIMO radar for advanced driver-assistance systems and autonomous driving: Advantages and challenges," *IEEE Signal Processing Magazine*, vol. 37, no. 4, pp. 98–117, 2020.
- [2] S. Kulkarni, A. Thakur, S. Soni, A. Hiwale, M. H. Belsare, and A. B. Raj, "A comprehensive review of direction of arrival (DoA) estimation techniques and algorithms," *Journal of Electronics and Electrical Engineering*, pp. 138–186, 2025.
- [3] G. Jekateryńczuk and Z. Piotrowski, "A survey of sound source localization and detection methods and their applications," *Sensors*, vol. 24, no. 1, p. 68, 2023.
- [4] S. Zang, M. Ding, D. Smith, P. Tyler, T. Rakotoarivelo, and M. A. Kaafar, "The impact of adverse weather conditions on autonomous vehicles: How rain, snow, fog, and hail affect the performance of a self-driving car," *IEEE Vehicular Technology Magazine*, vol. 14, no. 2, pp. 103–111, 2019.
- [5] H. Wallace, "Millimeter-wave propagation measurements at the ballistic research laboratory," *IEEE Transactions on Geoscience and Remote Sensing*, vol. 26, no. 3, pp. 253–258, 1988.
- [6] C. Yan, G. Leus, and M. Bengtsson, "Robust covariance-based DoA estimation under weather-induced distortion," in *Proc. 59th Asilomar Conf. Signals, Systems, and Computers*, Pacific Grove, CA, USA, 2025, accepted for publication (to appear). Preprint submitted to arXiv.
- [7] B. Yektakhab and K. Sarabandi, "A model for the statistics of field fluctuation, phase front aberration, and field spatial covariance of electromagnetic waves propagating in rain," *IEEE Transactions on Antennas and Propagation*, vol. 72, no. 3, pp. 2755–2765, 2024.
- [8] W. Liu, "Super resolution DoA estimation based on deep neural network," *Scientific reports*, vol. 10, no. 1, p. 19859, 2020.
- [9] G. K. Papageorgiou, M. Sellathurai, and Y. C. Eldar, "Deep networks for direction-of-arrival estimation in low SNR," *IEEE Transactions on Signal Processing*, vol. 69, pp. 3714–3729, 2021.
- [10] J. P. Merkofer, G. Revach, N. Shlezinger, T. Routtenberg, and R. J. Van Sloun, "DA-MUSIC: Data-driven DoA estimation via deep augmented MUSIC algorithm," *IEEE Transactions on Vehicular Technology*, vol. 73, no. 2, pp. 2771–2785, 2023.
- [11] N. Shlezinger, J. Whang, Y. C. Eldar, and A. G. Dimakis, "Model-based deep learning," *Proceedings of the IEEE*, vol. 111, no. 5, pp. 465–499, 2023.
- [12] R. Yang, Y. Hu, S. Sun, and Y. D. Zhang, "Advancing subspace representation learning for DOA estimation using sparse arrays," in *Proceedings of the 59th Annual Asilomar Conference on Signals, Systems, and Computers*, Pacific Grove, CA, USA, Oct. 2025.
- [13] Y. Hu, S. Sun, and Y. D. Zhang, "Model-based learning for DOA estimation with one-bit single-snapshot sparse arrays," *IEEE Journal of Selected Topics in Signal Processing*, vol. 19, no. 6, pp. 909–925, 2025.
- [14] J. Hammersley, *Monte Carlo Methods*. Springer Science & Business Media, 2013.
- [15] A. Kendall, Y. Gal, and R. Cipolla, "Multi-task learning using uncertainty to weigh losses for scene geometry and semantics," in *Proceedings of the IEEE conference on Computer Vision and Pattern Recognition (CVPR)*, 2018, pp. 7482–7491.